Title	Tailoring oxygen sensing characteristics of Co_3O_4 nanostructures through Gd doping
Author(s)	S. Fareed, R. Medwal, Joseph Vimal Vas, Ijaz A. Khan, Rajdeep Singh Rawat and M. A. Rafiq
Source	*Ceramics International*, *46*(7), 9498-9506
Published by	Elsevier

Tailoring oxygen sensing characteristics of Co_3O_4 nanostructures through Gd doping

S. Fareed[a,b], R. Medwal[b], Joseph Vimal Vas[b], Ijaz A. Khan[b], Rajdeep Singh Rawat[*,b] and M. A. Rafiq[*,c]

[a] Department of Metallurgy and Materials Engineering, Pakistan Institute of Engineering and Applied Sciences (PIEAS), P.O. Nilore, Islamabad, 45650, Pakistan

[b] Natural Science and Science Education, National Institute of Education, Nanyang Technological University, Singapore 637616

[c] Department of Physics and Applied Mathematics, Pakistan Institute of Engineering and Applied Sciences (PIEAS), P.O. Nilore, Islamabad, 45650, Pakistan

Abstract

Detection of oxygen plays an important role in food industry, medicine and controlling automotive exhaust. Here, we have developed a Co_3O_4 nanoparticle-based oxygen gas sensor. Effect of Gadolinium (Gd) doping on oxygen sensing is investigated using the variation in electrical resistance method which clearly reveals improvement in the sensitivity with the increase in Gadolinium doping in Co_3O_4. X-ray diffraction (XRD), Scanning electron microscopy (SEM), Transmission electron microscopy (TEM) and X-ray photoelectron spectroscopy (XPS) studies were systematically performed, to understand the effect of the morphology and crystallographic phase on the level of sensitivity with Gadolinium doping. XRD studies reveal a distortion in the Co_3O_4 lattice as the lattice parameters with increase with increasing Gd doping. SEM and TEM show a change in particle shape and size with Gd doping. Presence of both Co^{+2} and Co^{+3} oxidation states were confirmed by XPS. Gd doping, up to 6%, improved the gas sensing response of Co_3O_4 nanoparticles which is attributed to the decrease in particle size and an increase in oxygen adsorption with Gd doping. Minimum response time of 4 s, 6 s, 10 s and 14 s were observed for pure Co_3O_4 in 1%, 2%, 3% and 4% oxygen environment respectively. Pure Co_3O_4 nanoparticles also showed minimum recovery time which was 6 s, 7 s, 9 s and 11 s in 1%, 2%, 3% and 4%

oxygen environment respectively. All the prepared compositions were selective to oxygen at 240 °C.

Key Words
Gd doped Co_3O_4, nanoparticles, co-precipitation, oxygen sensor, chemiresistive sensor

Introduction:

Gas sensing properties of semiconductor metal oxides have been extensively investigated in the last decade due to their high sensitivity, low cost, feasibility of miniaturization and longer life time[1–3]. Detection of oxygen is important to monitor and control many industrial processes like fermentation process, food and beverage packaging and chemical processing. Semiconductor metal oxides are potential materials to be used in such industries. n-type semiconductors have been widely investigated as gas sensitive material. However due to their high cross sensitivity to humidity, they are difficult to use in actual environmental conditions. On the other hand, p-type semiconducting materials such as NiO, Mn_3O_4, CuO and Co_3O_4 are characterized by higher capacity to chemisorb oxygen [4], and higher catalytic activity in oxidation reactions [5] which make them promising materials for detecting gases in environmental conditions [6].

Long term stability of semiconductor metal oxides sensors, however, is inadequate due to their higher operating temperatures [7]. In recent years, the sensing performance of metal-oxide based sensors has been enhanced using nanostructured morphologies and modulating the size of the nanoparticles by doping with suitable materials [8,9]. Sensitivity of metal oxide based gas sensors have also been enhanced by using the strategies such as functionalization with noble metals, by using the oxide heterostructures and thermal assistance [10,11]. It has been observed that the creation of oxygen vacancies in semiconductor metal oxides facilitate the adsorption of oxygen on the metal oxide surface which can increase the response of a semiconductor gas sensor [12]. One

of the preferred technique for the incorporation of oxygen vacancies in metal oxide semiconductors is the doping [13]. The creation of oxygen vacancies in semiconductor metal oxides by doping motivated the idea of using the p-type semiconductor metal oxide and dope it with suitable material to create oxygen vacancies to enhance its response towards oxygen gas. Creation of oxygen vacancies in p-type semiconductor metal oxide may increase the response values of these gas sensors. Low cross sensitivity of p-type gas sensors towards humidity combined with the higher response values may make these materials useful for gas sensing applications.

Cobalt oxide (Co_3O_4) is one of the versatile p-type semiconductor metal oxides. It has cubic fcc lattice with spinel structure containing Co^{+2} and Co^{+3} oxidation states at different lattice points. In Co_3O_4 lattice, one half of the octahedral sites are occupied by Co^{+3} ions whereas one eighth of the tetrahedral sites are occupied by Co^{+2} ions [14,15]. It has a band gap of 1.6-2.2 eV [16]. p-type behavior in Co_3O_4 is supposed to be due to the metal vacancies in the crystal lattice [14].

Co_3O_4 has been investigated for the sensing of methanol, ethanol [17], NH_3 [18], acetone [19], NOx [20], H_2S [21], CO [22], etc. However, its potential to detect oxygen has been neglected because of the lower response value. Creation of oxygen deficient regions can result in an increase in its response towards oxygen by providing sites for oxygen adsorption [23]. In this research work we have used the novel idea of using doping technique to create oxygen vacancies in p-type Co_3O_4 nanostructures and to study the effect of doping on the oxygen sensing characteristics of Co_3O_4. Novelty of this work was to use Gd as a dopant to tailor the oxygen sensing characteristics of Co_3O_4 nanostructures which to the best of our knowledge have not been studied yet. Co_3O_4 nanoparticles with different doping concentrations of Gd, (0, 3, 6 and 9 atomic%), were prepared using a coprecipitation method and their oxygen sensing characteristics were studied above room temperature to get appreciable response values.

Materials and Methods:

$Co(NO_3)_2.6H_2O$ (99%) and $Gd(NO_3)_3.6H_2O$ (99.9%), purchased from Sigma Aldrich, were used as reagents for the preparation of pure and Gd doped Co_3O_4 nanoparticles. Coprecipitation method followed by calcination was used for the fabrication of nanoparticles. Desired molar ratios of $Co(NO_3)_2.6H_2O$ and $Gd(NO_3)_3.6H_2O$ were dissolved in deionized (DI) water at room temperature (25 ℃). Hydroxide particles of all the compositions were precipitated by drop wise addition of one molar NaOH solution into the prepared aqueous solution. The precipitates formed were washed successively with DI water and then with ethanol several times to ensure complete removal of impurity ions. After washing, the precipitates were dried in an oven at 80 ℃ for 24 hours followed by calcination at 600 ℃ for 6 hours. Prepared powders were characterized for structure by using X-ray diffraction (XRD) technique using Siemens D5000. The morphology of the prepared nanostructures was studied using Scanning Electron Microscopy (SEM) (FESEM 6340F) and Transmission Electron Microscopy (TEM) (JEOL 2010 HR). Modes of vibration in prepared powders were studied using Raman Spectroscopy (Renishaw inVia). Chemical states of Gd, Co, and O in Gd doped Co_3O_4 nanoparticles were determined by using X-ray Photoelectron Spectroscopy (XPS) technique (Kratos AXIS Supra).

Results and Discussions:

Structural characterization of the prepared Co_3O_4 nanoparticles was carried out using a Siemens X-ray diffractometer using Cu-K_α radiation (λ=1.5406 Å) at a scan speed of 0.1 degrees/min. Figure 1(a) shows XRD patterns of pure and Gd doped cobalt oxide nanoparticles. XRD pattern of pure cobalt oxide matched with the JCPDS card number 01-074-1656 corresponding to Co_3O_4 with cubic structure having Fd3m space group. No additional peak corresponding to any impurity phase was observed in XRD pattern of undoped Co_3O_4. With Gd doping in Co_3O_4 there is a slight

shift in XRD peak positions towards lower 2θ values indicating an increase in lattice parameters. 2θ values of (311) plane and lattice parameter calculated from (311) are shown in figure 1(b). Increase in lattice parameters of Co_3O_4 is expected due to the substitution of larger sized Gd^{+3} (0.93 Å) ions in the lattice position of smaller Co^{+3} (0.53 Å) ions [24]. Minor peaks of Gd_2O_3 are also observed in 9% Gd doped nanoparticles showing the formation of Co_3O_4-Gd_2O_3 mixed phase. The average crystallite size decreased with the doping of Gd as calculated by Scherrer formula to the most intense (311) diffraction peak of Co_3O_4. Calculated values of crystallite size are 56.7 nm, 25.7 nm, 17.1 nm and 16.6 nm for pure, 3% Gd-, 6% Gd- and 9% Gd-doped samples respectively. Substitution of an ion in the lattice with a larger sized ion induces strain in the lattice. With increasing dopant concentration, the dopants are accommodated on the grain or crystallite surface to minimize the strain. As a result of the segregation of dopants on the surface, the surface to volume ratio needs to be increased to minimize the energy of the lattice. As a result the crystallite size is reduced with doping [25].

The morphology of the prepared nanostructure was studied using SEM. Particles were coated with gold by using DC sputtering coating unit (JEOL) before SEM measurements to avoid the charging effect. Figures 2(a-d) show SEM images of the pure and Gd-doped Co_3O_4 nanostructures. SEM images indicate that the fabricated nanoparticles are composed of aggregates of smaller particles. The morphology of pure Co_3O_4, as seen in figure 2(a), appears to consist of more uniform-shaped larger-sized plate-like nanostructures. The morphology of Gd-doped Co_3O_4 changes into non-uniform fragmented reduced-sized nano-plates. Nanoparticles aggregate during precipitation from the solution due to nanoscale forces between them. With the addition of dopant, the combined effect of van der Waals forces and electrostatic interactions between the particles promotes the self-aggregation of nanoparticles to form nano plates [26]. Average size of nano-plates on Gd

doped samples is significantly smaller, with larger non-uniform sizes and shapes distributions, than in the pure Co_3O_4. Typical values of average nanoplate sizes are ~128 nm, ~106 nm, ~96 nm and ~87 nm for pure, 3% Gd-, 6% Gd- and 9% Gd-doped Co_3O_4 samples.

Figures 3(a-d) show TEM images of the as-prepared nanostructures. TEM images also clearly indicate a change in the morphology of nanostructures with Gd doping. The larger-sized relatively more uniform bigger sized nanoplates in figure 3a for pure Co_3O_4 are seen to fragment into smaller-sized relatively more non-uniform nanoplates or nanosheets in figure 3(b-d). Insets in figure 3 show high resolution TEM (HR-TEM) and selected area electron diffraction (SAED) patterns of fabricated nanostructures. HR-TEM images, inset in figure 3a, c & d, show an increase in lattice spacing along (111) planes from 0.452 nm in pure Co_3O_4 to 0.462 and 0.471 nm for 3% and 9 % Gd-doped Co_3O_4. SAED patterns of the prepared nanostructures clearly indicate that the fabricated particles are polycrystalline in nature.

Modes of vibration of a material can be identified by using Raman spectroscopy. Since the phonon vibrations are sensitive towards addition of impurity atoms in the host material. Raman spectroscopy can be used for the identification of dopants. Raman spectra of Cobalt oxide before and after doping were obtained in the 300 cm^{-1} to 1000 cm^{-1} range and are shown in figure 4. Pure Co_3O_4 depicts four prominent Raman bands at 481, 520, 616 and 690 cm^{-1}. The two main peaks, located at 481 cm^{-1} and 690 cm^{-1} represent the Raman active modes E_g and A_{1g}, respectively. Peaks at 520 cm^{-1} and 616 cm^{-1} represent the $F_{2g}(2)$ and $F_{2g}(1)$ symmetry, respectively [27,28]. Addition of Gd has led the Raman active mode peaks located at 481 cm^{-1} (Eg) and 690 cm^{-1} (A1g) in pure Co_3O_4 to shift to 475 cm^{-1} and 679 cm^{-1} respectively in 9% Gd doped Co_3O_4. This peak shift was also associated with the peak broadening. The addition of Gd into cobalt oxide produces a tensile stress which not only shifted the peaks towards lower values but also deteriorated the crystallinity.

XPS spectra obtained were calibrated to C1s binding energy peak at 284.8 eV. Figures 5 (a-c) show the high resolution core level XPS spectra of Co (2p), O (1s) and Gd (4d), respectively. Two cobalt peaks corresponding to $Co(2p_{3/2})$ and $Co(2P_{1/3})$ are observed in XPS spectra as shown in figure 5a[29]. Asymmetric Co XPS peaks are deconvoluted into Co^{+2} and Co^{+3} peaks. Peaks at binding energy of 779.6 eV and 794.36 eV are of Co^{+3} oxidation state whereas peaks at binding energy of 780.8 eV and 796.1 eV are of Co^{+2} oxidation state. Satellite peaks observed at a binding energy of 786.3 eV may be due to surface Co^{+2} species [30]. XPS spectra of Cobalt confirms the presence of both Co^{+2} and Co^{+3} oxidation states in the prepared nanoparticles which is in agreement with the structure of Co_3O_4 as observed in XRD results.

O(1s) spectra, in figure 5b, were deconvoluted into two peaks corresponding to lattice oxygen at a binding energy of 529.5 eV and oxygen defects or oxygen vacancies at a binding energy of 531.2 eV [29]. The stoichiometric ratio of lattice oxygen and oxygen vacancies can be estimated from the peak ratios. The peak areas due to oxygen defects or vacancies increased from 39% for pure Co_3O_4 to 59% for 6% Gd doped Co_3O_4. The increase in the peak area indicates an increase in oxygen vacancies with Gd doping and favoring the formation of $Co_3O_{4-\delta}$ [31]. Figure 5c illustrates Gd(4d) high resolution XPS spectra of pure and Gd-doped Co_3O_4. Observed binding energy peaks are asymmetric and fitted into two peaks corresponding to $Gd(4d_{5/2})$ at a binding energy of 141.7 eV and $Gd(4d_{3/2})$ at a binding energy of 147.5eV [32]. Gd peaks observed in high resolution XPS spectra confirm the presence of Gd in the lattice of Co_3O_4.

To study the oxygen sensing characteristics of the prepared compositions, the prepared powder samples were formed into pellets with diameter of 20 mm by uniaxially applying 4 Ton load. Two electrical contacts were made on the same side of pellets using silver paste. Distance between the electrical contacts was 10 mm. For sensing measurements, the pellet was placed in a vacuum

chamber and electrically connected to an Agilent 4156C parameter analyzer. Then the chamber was evacuated by means of a vacuum pump. After evacuating the chamber, it was filled with nitrogen gas (99.99 %) at a pressure of 1 atmosphere. Different concentrations of oxygen mixed in nitrogen were introduced into the chamber and the resistance of the pellet was monitored at 1 V DC. Concentration of each gas in the mixture was controlled through "ALICAT" mass flow controllers. When oxygen entered the chamber, the resistance of all the prepared sensors started decreasing due to the p-type conductivity of Co_3O_4. The chamber also had the arrangement to change the temperature of the sensor. Different concentrations of oxygen (1%, 2%, 3% and 4%) were introduced into the chamber and the response was measured by using the relations:

$$Response\ (\%) = \frac{R_a - R_g}{R_a} \times 100$$

Here R_a is the resistance of the sample in 1 atmosphere of nitrogen and R_g is the resistance of sample in test gas.

Figure 6 shows the response of the sensors as a function of temperature in 4% Oxygen concentration. Gd doped sensors showed a maximum response at 240 ℃. Therefore, the sensing characteristics of all the sensors were later determined at 240 ℃. Figures 7(a-d) show transient response recovery curves of all the prepared sensor samples in 1%, 2%, 3% and 4% oxygen concentration at 240 ℃. The response of the sensors increased as the oxygen entered in to the test chamber and reached a stable point after some time and dropped again to baseline (zero) level as the oxygen was removed. Figure 8(a) shows the response as a function of the oxygen concentration for all the prepared sensors. Pure Co_3O_4 nanoplates sensor showed lowest response towards oxygen gas that was 17%, 35%, 77% and 107% in 1%, 2%, 3% and 4% oxygen concentration respectively. Doping of Gd in Co_3O_4 nanoparticles increased the sensor response as can be seen

for the 3% Gd doped Co_3O_4 nanoparticles sensor. Response of the 3% Gd doped Co_3O_4 nanoparticles sensor increased to 48%, 133%, 364% and 572% for 1%, 2%, 3% and 4% oxygen concentration respectively. Increasing the Gd-doping concentration to 6% increased the response of the sensor further to 227%, 471%, 696% and 921% in 1%, 2%, 3% and 4% oxygen environment respectively. With further addition of Gd into Co_3O_4 nanoparticles, the response decreased to 193%, 408%, 552%, and 711% in 1%, 2%, 3% and 4% oxygen concentration respectively for 9% Gd doped Co_3O_4 nanoparticles sensor. Response time is considered as the time taken by the sensors to give 90% of the full-scale reading. Response time of all the prepared nanoparticles sensors were determined from figures 7(a-d) and are represented in figure 8(b). Figure 8(b) represents the oxygen concentration dependent response time of all the prepared nanoparticles sensors. Minimum response time of 4 s, 6 s, 10 s and 14 s were observed for pure Co_3O_4 in 1%, 2%, 3% and 4% oxygen environment respectively. The response time of the sensors increased with the addition of Gd in the Co_3O_4 nanostructures. The maximum response time was observed for nanoparticles doped with 9% Gd amounting to 20 s, 22 s, 23 s and 26 s for response in 1%, 2%, 3% and 4% oxygen concentration respectively.

Recovery time was calculated as the time taken by the sensor to revert back to 90% of its original resistance value after the evacuation of the test gas. Figure 8(c) represents the recovery time of the prepared nanoparticles sensors. Minimum recovery time was observed for pure Co_3O_4 nanoparticles sensors. Recovery time also increased with increasing Gd doping into Co_3O_4 up to 6% Gd doping. With further increasing the Gd doping above 6%, recovery time started decreasing.

Figure 9(a-d) depicts the continuity of response recovery transient in 4% oxygen environment at 240 ℃. Figure 10 depicts the stability of the response in 4% oxygen concentration at 240 ℃ for up to 28 days. Figure 10 shows that the response of all the sensors was stable with less than 5%

change during the trial period of 28 days. The prepared sensors were tested in 4% concentration of methanol, ethanol, propanol and acetone at 240 ℃ and the result is presented in Figure 11. Figure 11 depicts that all the prepared sensors were selective to oxygen at 240 ℃.

Comparison of oxygen sensing characteristics of Gd doped Co_3O_4 nanoparticles with other metal oxides is given in Table I.

Table I Gd doped Co3O4 oxygen sensing characteristics comparison with different metal oxides

Material	**Response (%)**	**Response Time (s)**	**Recovery Time (s)**	**Ref**
$NiFe_2O_4$ nanoparticles	5.33 (1000 ppm)	600	240-360	[33]
$LaFeO_3$ nanoparticles	20 (2% oxygen)	8	12	[34]
TiO_2/Graphene	27 (100% oxygen)	193	135	[35]
Pt doped In_2O_3 nanoparticles	3.8 (20 % oxygen)	40	45	[36]
6% Gd doped Co_3O_4 nanoparticles	921 (4 % oxygen)	23	22	This study

Gas sensing mechanism in Co_3O_4 nanostructures involves the resistance change associated with the adsorption and desorption of oxygen species on the surface of the nanoparticles. When the oxygen enters the test chamber, it is adsorbed on the surface of sensor in the form of different species depending upon the temperature by the following reactions [37,38]:

$$O_2(gas) + e^- \leftrightarrow O_2^-(adsorb) \qquad (< 100\ ℃)$$

$$O_2(gas) + 2e^- \leftrightarrow 2O^-(adsorb) \qquad (100 - 300\ ℃)$$

$$O_2(gas) + 4e^- \leftrightarrow 2O^{2-}(adsorb) \qquad (> 300\ ℃)$$

Due to the adsorption of oxygen on p-type Co_3O_4, electrons from the valence band are promoted to the adsorbing oxygen by thus generating holes in the valence band thereby increasing the hole concentration and thus decreasing the resistance of the p-type semiconductor. This adsorption of oxygen on the surface of p-type oxides creates hole accumulation layer on the surface of the

nanostructured sensors [38]. Increasing oxygen concentrations will cause more oxygen to adsorb on the surface thus resulting in a widening the hole accumulation layer thereby decreasing the sensor resistance and increasing the sensor response with increasing oxygen concentration. As can be seen from XPS results, incorporation of Gd into Co_3O_4 nanoparticles increased the oxygen vacancies. Oxygen vacancies have been proved to be an effective method to enhance the gas sensing performance [39,40]. Oxygen vacancies provide more active sites for the oxygen adsorption thereby increasing the response. Another reason for the improved gas sensing efficiency is the increase in the oxygen adsorption surface area of sensor. As seen from the SEM and TEM results the average size and shape-uniformity of the Co_3O_4 nanoplates was significantly reduced with the increasing Gd-doping concentration. This leads to an increase in the total available surface area for oxygen adsorption with increasing Gd-doping. This increase in the area of the nanostructures together with the increased Gd content (which increases the density of oxygen deficient sites) should result in an increased oxygen sensing performance. However, as noticed, the increase in the Gd-doping to 9% resulted in the formation of Gd_2O_3. Formation of Gd_2O_3 may have decreased the Gd content in the Co_3O_4 nanostructures which has resulted net over-riding effect of decrease of sensor response at 9% Gd doping.

Conclusions

In this work Gd doped cobalt oxide nanoparticles were successfully synthesized and their oxygen sensing characteristics were studied. XRD analysis confirmed the formation of Co_3O_4 nanoparticles having cubic symmetry. Average nanoplates size and shape uniformity decreased with Gd doping. Increase in the response of sensors towards oxygen was observed up to 6% Gd doping. All the prepared sensors were stable with less than 5% change in response during the studied period of 28 days. Pure and Gd doped Co_3O_4 sensors were also selective to oxygen at 240

°C. Increase in response towards oxygen may be attributed to the increase in oxygen adsorption due to decrease in average nanoplates size and the formation of oxygen vacancies due to the increased Gd content.

Bibliography

[1] N. Barsan, D. Koziej, U. Weimar, Metal oxide-based gas sensor research: How to?, Sensors Actuators B Chem. 121 (2007) 18–35. doi:10.1016/J.SNB.2006.09.047.

[2] C. Wang, L. Yin, L. Zhang, D. Xiang, R. Gao, C. Wang, L. Yin, L. Zhang, D. Xiang, R. Gao, Metal Oxide Gas Sensors: Sensitivity and Influencing Factors, Sensors. 10 (2010) 2088–2106. doi:10.3390/s100302088.

[3] Y.-F. Sun, S.-B. Liu, F.-L. Meng, J.-Y. Liu, Z. Jin, L.-T. Kong, J.-H. Liu, Y.-F. Sun, S.-B. Liu, F.-L. Meng, J.-Y. Liu, Z. Jin, L.-T. Kong, J.-H. Liu, Metal Oxide Nanostructures and Their Gas Sensing Properties: A Review, Sensors. 12 (2012) 2610–2631. doi:10.3390/s120302610.

[4] M. Iwamoto, Y. Yoda, N. Yamazoe, T. Seiyama, Study of metal oxide catalysts by temperature programmed desorption. 4. Oxygen adsorption on various metal oxides, J. Phys. Chem. 82 (1978) 2564–2570. doi:10.1021/j100513a006.

[5] S. Royer, D. Duprez, Catalytic Oxidation of Carbon Monoxide over Transition Metal Oxides, ChemCatChem. 3 (2011) 24–65. doi:10.1002/CCTC.201000378.

[6] S. Vladimirova, V. Krivetskiy, M. Rumyantseva, A. Gaskov, N. Mordvinova, O. Lebedev, M. Martyshov, P. Forsh, Co3O4 as p-type material for CO sensing in humid air, Sensors (Switzerland). 17 (2017). doi:10.3390/s17102216.

[7] D. Selvakumar, N. Dharmaraj, N.S. Kumar, V.C. Padaki, Oxygen sensing properties of

platinum doped indium oxide nanoparticles prepared by hydrothermal method, Synth. React. Inorganic, Met. Nano-Metal Chem. 45 (2014) 753–758. doi:10.1080/15533174.2013.843548.

[8] M.A. Basyooni, M. Shaban, A.M. El Sayed, Enhanced Gas Sensing Properties of Spin-coated Na-doped ZnO Nanostructured Films, Sci. Rep. 7 (2017) 41716. doi:10.1038/srep41716.

[9] K. Sankarasubramanian, P. Soundarrajan, T. Logu, K. Sethuraman, K. Ramamurthi, Enhancing resistive-type hydrogen gas sensing properties of cadmium oxide thin films by copper doping, New J. Chem. 42 (2018) 1457–1466. doi:10.1039/c7nj03095a.

[10] J. Zhang, X. Liu, G. Neri, N. Pinna, Nanostructured Materials for Room-Temperature Gas Sensors, Adv. Mater. 28 (2016) 795–831. doi:10.1002/adma.201503825.

[11] N. Joshi, T. Hayasaka, Y. Liu, H. Liu, O.N. Oliveira, L. Lin, A review on chemiresistive room temperature gas sensors based on metal oxide nanostructures, graphene and 2D transition metal dichalcogenides, Microchim. Acta. 185 (2018). doi:10.1007/s00604-018-2750-5.

[12] J. Liu, Y. Gao, X. Wu, G. Jin, Z. Zhai, H. Liu, Inhomogeneous oxygen vacancy distribution in semiconductor gas sensors: Formation, migration and determination on gas sensing characteristics, Sensors (Switzerland). 17 (2017). doi:10.3390/s17081852.

[13] A. Sarkar, G.G. Khan, The formation and detection techniques of oxygen vacancies in titanium oxide-based nanostructures, Nanoscale. 11 (2019) 3414–3444. doi:10.1039/c8nr09666j.

[14] S. Vetter, S. Haffer, T. Wagner, M. Tiemann, Nanostructured Co3O4 as a CO gas sensor: Temperature-dependent behavior, Sensors Actuators, B Chem. 206 (2015) 133–138. doi:10.1016/j.snb.2014.09.025.

[15] H.K. Lin, H.C. Chiu, H.C. Tsai, S.H. Chien, C. Bin Wang, Synthesis characterization and catalytic oxidation of carbon monoxide over cobalt oxide, Catal. Letters. 107 (2006) 223–230. doi:10.1007/s10562-005-0002-x.

[16] B. Varghese, B. Mukherjee, K.R.G. Karthik, K.B. Jinesh, S.G. Mhaisalkar, E. Soon Tok, C. Haur Sow, Electrical and photoresponse properties of Co $_3$ O $_4$ nanowires, J. Appl. Phys. 111 (2012) 104306. doi:10.1063/1.4712497.

[17] W. Tan, J. Tan, L. Li, M. Dun, X. Huang, Nanosheets-assembled hollowed-out hierarchical Co3O4microrods for fast response/recovery gas sensor, Sensors Actuators, B Chem. 249 (2017) 66–75. doi:10.1016/j.snb.2017.04.068.

[18] Z. Li, W. Liu, Y.Q. Fu, J. Wang, Z. Lin, N. Wang, Z. Wang, K. Sun, High precision NH3 sensing using network nano-sheet Co3 O4 arrays based sensor at room temperature, Sensors Actuators B Chem. 235 (2016) 222–231. doi:10.1016/j.snb.2016.05.063.

[19] Y. Lin, H. Ji, Z. Shen, Q. Jia, D. Wang, Enhanced acetone sensing properties of Co3O4 nanosheets with highly exposed (111) planes, J. Mater. Sci. Mater. Electron. 27 (2016) 2086–2095. doi:10.1007/s10854-015-3995-y.

[20] T. Akamatsu, T. Itoh, N. Izu, W. Shin, NO and NO2 sensing properties of WO3 and Co3O4 based gas sensors, Sensors (Switzerland). 13 (2013) 12467–12481. doi:10.3390/s130912467.

[21] H.T. Long, N. Van Hieu, D.T.T. Le, P.L. Quang, N.D. Cuong, T.T. Hoa, C.M. Hung, Simple post-synthesis of mesoporous p-type Co3O4 nanochains for enhanced H2S gas sensing performance, Sensors Actuators B Chem. 270 (2018) 158–166. doi:10.1016/j.snb.2018.05.026.

[22] Z. Dou, C. Cao, Y. Chen, W. Song, Fabrication of porous Co3O4 nanowires with high CO sensing performance at a low operating temperature, Chem. Commun. 50 (2014) 14889–14891. doi:10.1039/c4cc05498a.

[23] J. Wu, Y. Yang, C. Zhang, H. Yu, L. Huang, X. Dong, J. Wang, X. Wang, Extremely sensitive and accurate H_2S sensor at room temperature fabricated with In-doped Co_3O_4 porous nanosheets, Dalt. Trans. (2019). doi:10.1039/C9DT01043B.

[24] R.G. Burns, The uptake of cobalt into ferromanganese nodules, soils, and synthetic manganese (IV) oxides, Geochim. Cosmochim. Acta. 40 (1976) 95–102. doi:10.1016/0016-7037(76)90197-6.

[25] A. Das, A.C. Mandal, S. Roy, P.M.G. Nambissan, Internal defect structure of calcium doped magnesium oxide nanoparticles studied by positron annihilation spectroscopy, AIP Adv. 8 (2018) 0–13. doi:10.1063/1.5001105.

[26] J. Judith Vijaya, G. Sekaran, M. Bououdina, Effect of Cu2+ doping on structural, morphological, optical and magnetic properties of MnFe2O4 particles/sheets/flakes-like nanostructures, Ceram. Int. 41 (2015) 15–26. doi:10.1016/j.ceramint.2013.10.145.

[27] J. Jiang, L. Li, Synthesis of sphere-like Co3O4 nanocrystals via a simple polyol route, Mater. Lett. 61 (2007) 4894–4896. doi:10.1016/j.matlet.2007.03.067.

[28] S. Farhadi, M. Javanmard, G. Nadri, Characterization of Cobalt Oxide Nanoparticles Prepared by the Thermal Decomposition, Acta Chim. Slov. 63 (2016) 335–343. doi:10.17344/acsi.2016.2305.

[29] L. Zhang, W. He, X. Xiang, Y. Li, F. Li, Roughening of windmill-shaped spinel Co3O4 microcrystals grown on a flexible metal substrate by a facile surface treatment to enhance their performance in the oxidation of water, RSC Adv. 4 (2014) 43357–43365. doi:10.1039/C4RA07082H.

[30] Y. Sun, J. Liu, J. Song, S. Huang, N. Yang, J. Zhang, Y. Sun, Y. Zhu, Exploring the Effect of Co3O4 Nanocatalysts with Different Dimensional Architectures on Methane Combustion, ChemCatChem. 8 (2016) 540–545. doi:10.1002/cctc.201501056.

[31] H.W. Kim, Y.J. Kwon, A. Mirzaei, S.Y. Kang, M.S. Choi, J.H. Bang, S.S. Kim, Synthesis of zinc oxide semiconductors-graphene nanocomposites by microwave irradiation for application to gas sensors, Sensors Actuators, B Chem. 249 (2017) 590–601. doi:10.1016/j.snb.2017.03.149.

[32] N. Zhang, D. Chen, F. Niu, S. Wang, L. Qin, Y. Huang, Enhanced visible light photocatalytic activity of Gd-doped BiFeO3 nanoparticles and mechanism insight, Sci. Rep. 6 (2016) 1–11. doi:10.1038/srep26467.

[33] R.B. Kamble, V.L. Mathe, Nanocrystalline nickel ferrite thick film as an efficient gas sensor at room temperature, Sensors Actuators, B Chem. 131 (2008) 205–209. doi:10.1016/j.snb.2007.11.003.

[34] I. Jaouali, H. Hamrouni, N. Moussa, M.F. Nsib, M.A. Centeno, A. Bonavita, G. Neri, S.G. Leonardi, LaFeO3 ceramics as selective oxygen sensors at mild temperature, Ceram. Int.

44 (2018) 4183–4189. doi:10.1016/j.ceramint.2017.11.221.

[35] J. Zhang, C. Zhao, P.A. Hu, Y.Q. Fu, Z. Wang, W. Cao, B. Yang, F. Placido, A UV light enhanced TiO2/graphene device for oxygen sensing at room temperature, RSC Adv. 3 (2013) 22185–22190. doi:10.1039/c3ra43480j.

[36] D. Selvakumar, N. Dharmaraj, N.S. Kumar, V.C. Padaki, Oxygen sensing properties of platinum doped indium oxide nanoparticles prepared by hydrothermal method, Synth. React. Inorganic, Met. Nano-Metal Chem. 45 (2014) 753–758. doi:10.1080/15533174.2013.843548.

[37] A.S.M. Iftekhar Uddin, D.T. Phan, G.S. Chung, Low temperature acetylene gas sensor based on Ag nanoparticles-loaded ZnO-reduced graphene oxide hybrid, Sensors Actuators, B Chem. 207 (2015) 362–369. doi:10.1016/j.snb.2014.10.091.

[38] B. Zhang, M. Cheng, G. Liu, Y. Gao, L. Zhao, S. Li, Y. Wang, F. Liu, X. Liang, T. Zhang, G. Lu, Room temperature NO 2 gas sensor based on porous Co 3 O 4 slices/reduced graphene oxide hybrid, Elsevier B.V., 2018. doi:10.1016/j.snb.2018.02.117.

[39] W. Shang, D. Wang, B. Zhang, C. Jiang, F. Qu, M. Yang, Aliovalent Fe(iii)-doped NiO microspheres for enhanced butanol gas sensing properties, Dalt. Trans. 47 (2018) 15181–15188. doi:10.1039/C8DT03242D.

[40] C. Wang, X. Cui, J. Liu, X. Zhou, X. Cheng, P. Sun, X. Hu, X. Li, J. Zheng, G. Lu, Design of Superior Ethanol Gas Sensor Based on Al-Doped NiO Nanorod-Flowers, ACS Sensors. 1 (2016) 131–136. doi:10.1021/acssensors.5b00123.

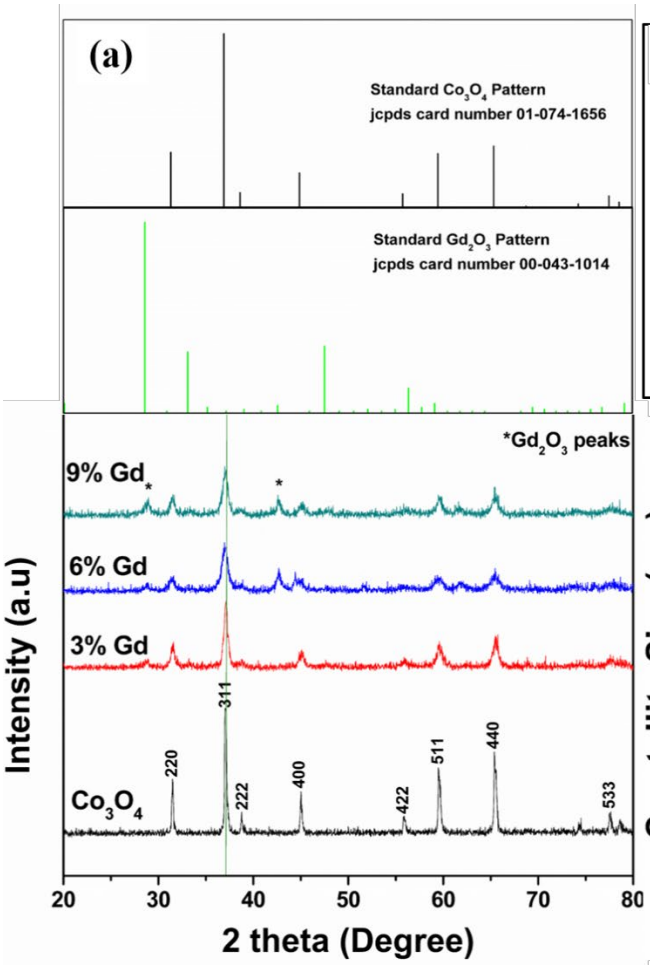

(b)

Composition	2 theta position of (311) plane (degree)	Lattice parameter (Å)
Pure Co_3O_4	37.06	8.04
3% Gd doping	37.01	8.05
6% Gd doping	36.93	8.07
9% Gd doping	36.87	8.09

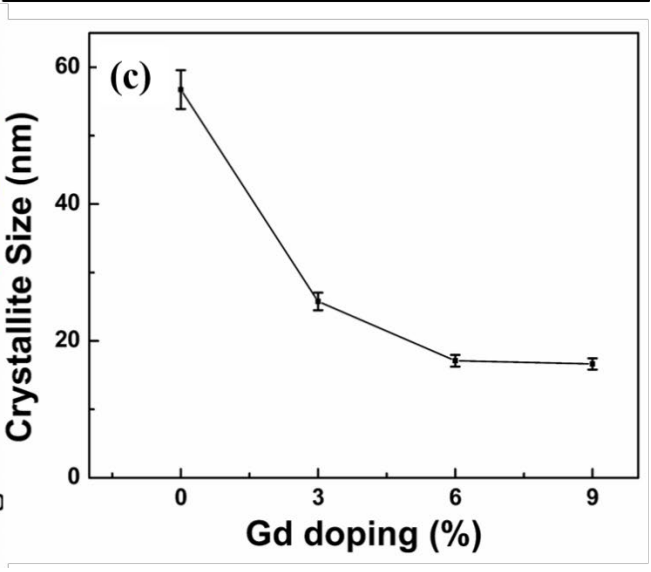

Figure 1 (a) XRD pattern of Co_3O_4, 3% Gd doped Co_3O_4, 6% Gd doped Co_3O_4 and 9% Gd doped Co_3O_4 (b) Effect of Gd doping on lattice parameter calculated using (311) plane (c) Effect of Gd doping on crystallite size

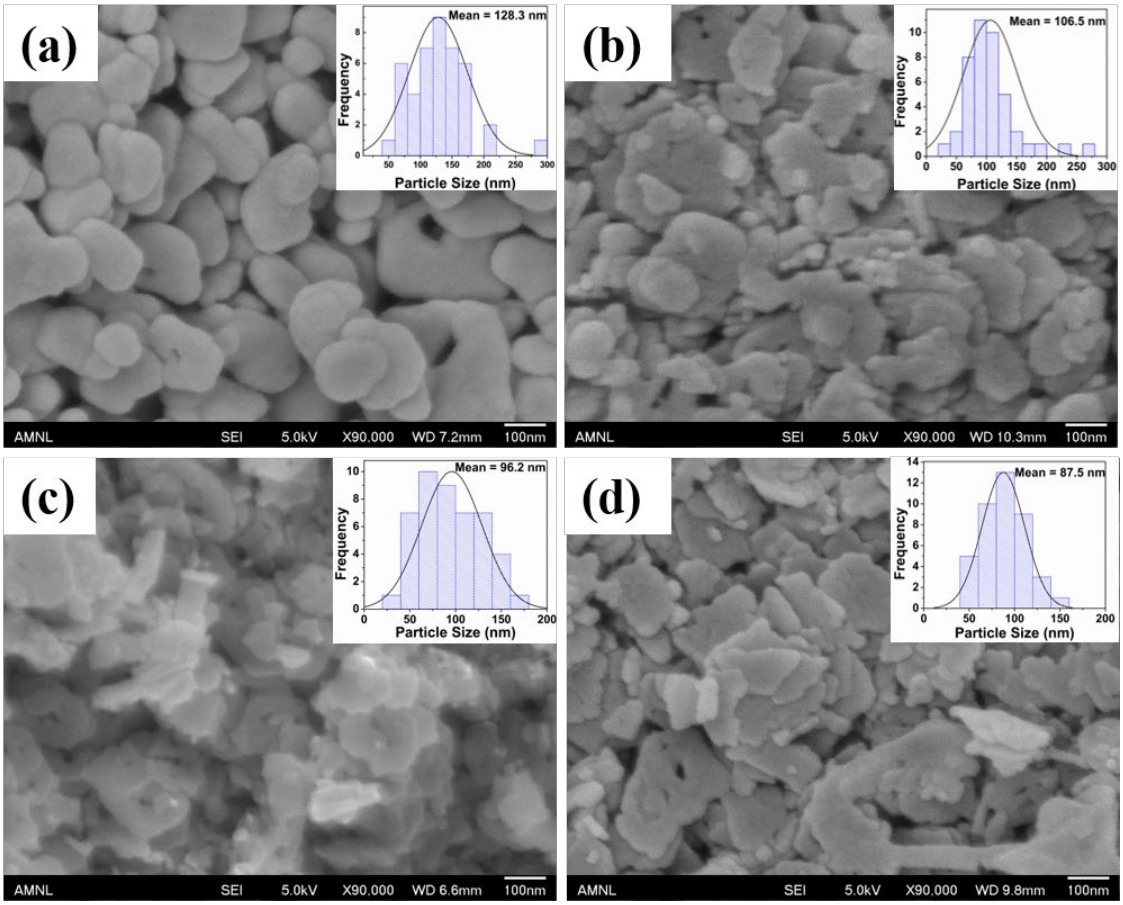

Figure 2 SEM image of (a) Co_3O_4 (b) 3% Gd doped Co_3O_4 (c) 6% Gd doped Co_3O_4 (d) 9% Gd doped Co_3O_4. Inset of the SEM images shows the particle size distribution.

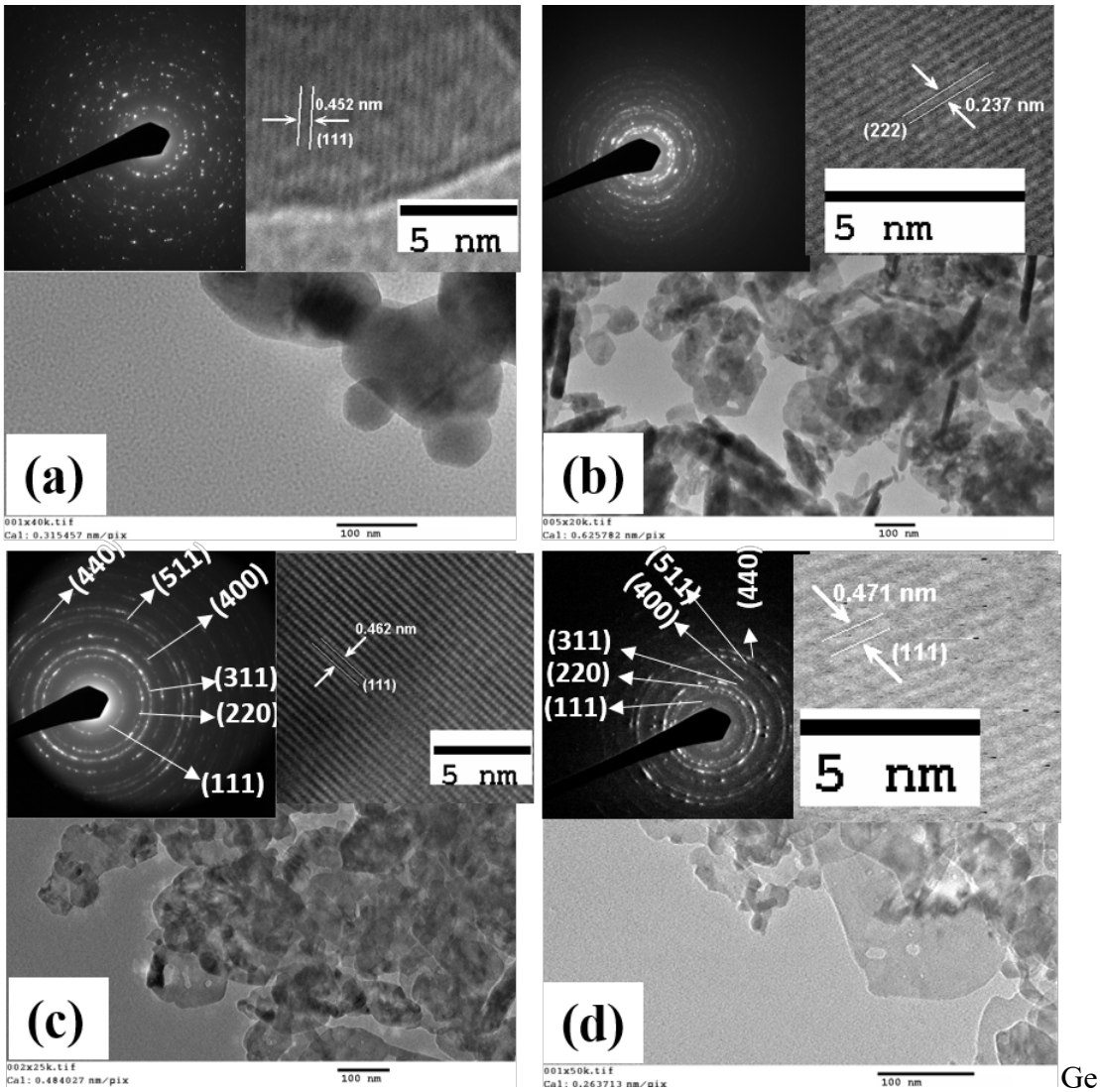

Figure 3 TEM image of (a) Co_3O_4 (b) 3% Gd doped Co_3O_4 (c) 6% Gd doped Co_3O_4 (d) 9% Gd doped Co_3O_4

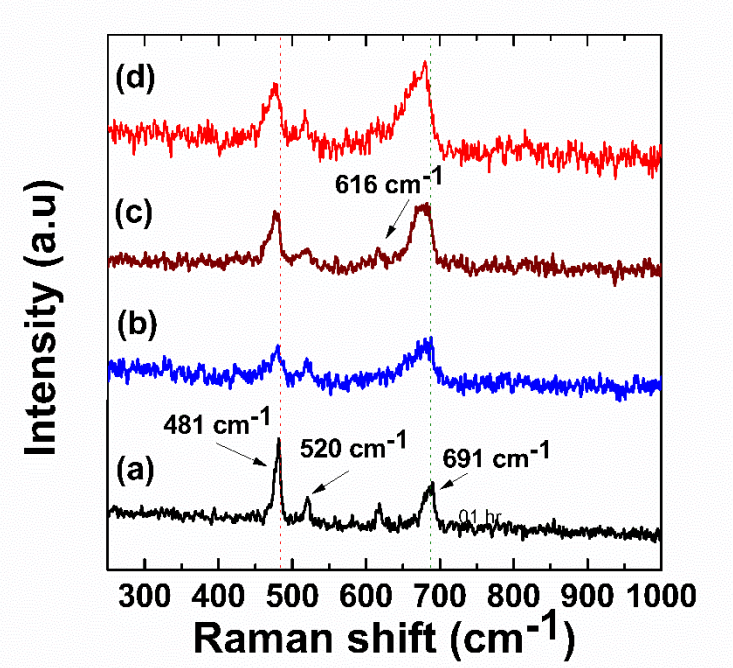

Figure 4 Raman shift in (a) pure Co_3O_4 (b) 3% Gd (c) 6% Gd and (d) 9%Gd doped Co_3O_4

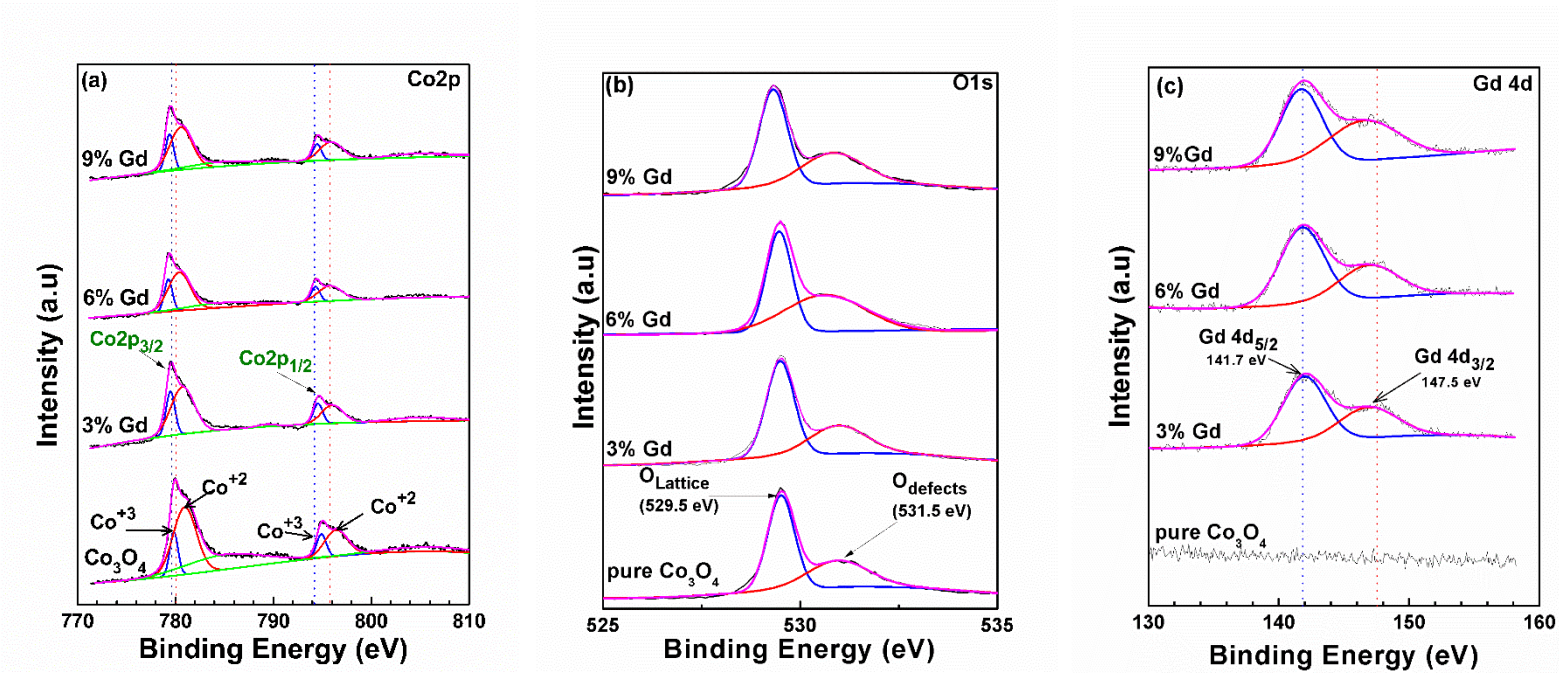

Figure 5 (a) Co2p (b) O1s and (c) Gd4d XPS spectra of pure Co_3O_4, 3%, 6% and 9% Gd doped Co_3O_4 nanoparticles

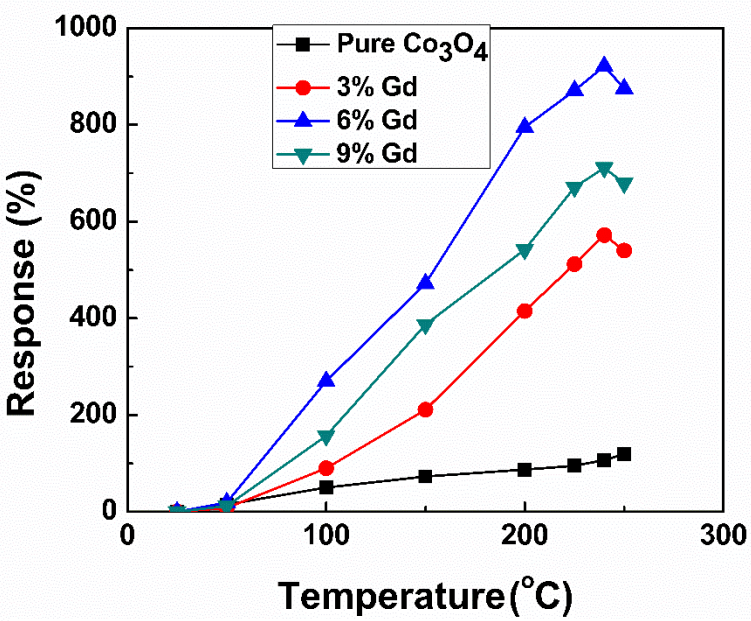

Figure 6 Temperature dependent response of sensors in 4% oxygen concentration

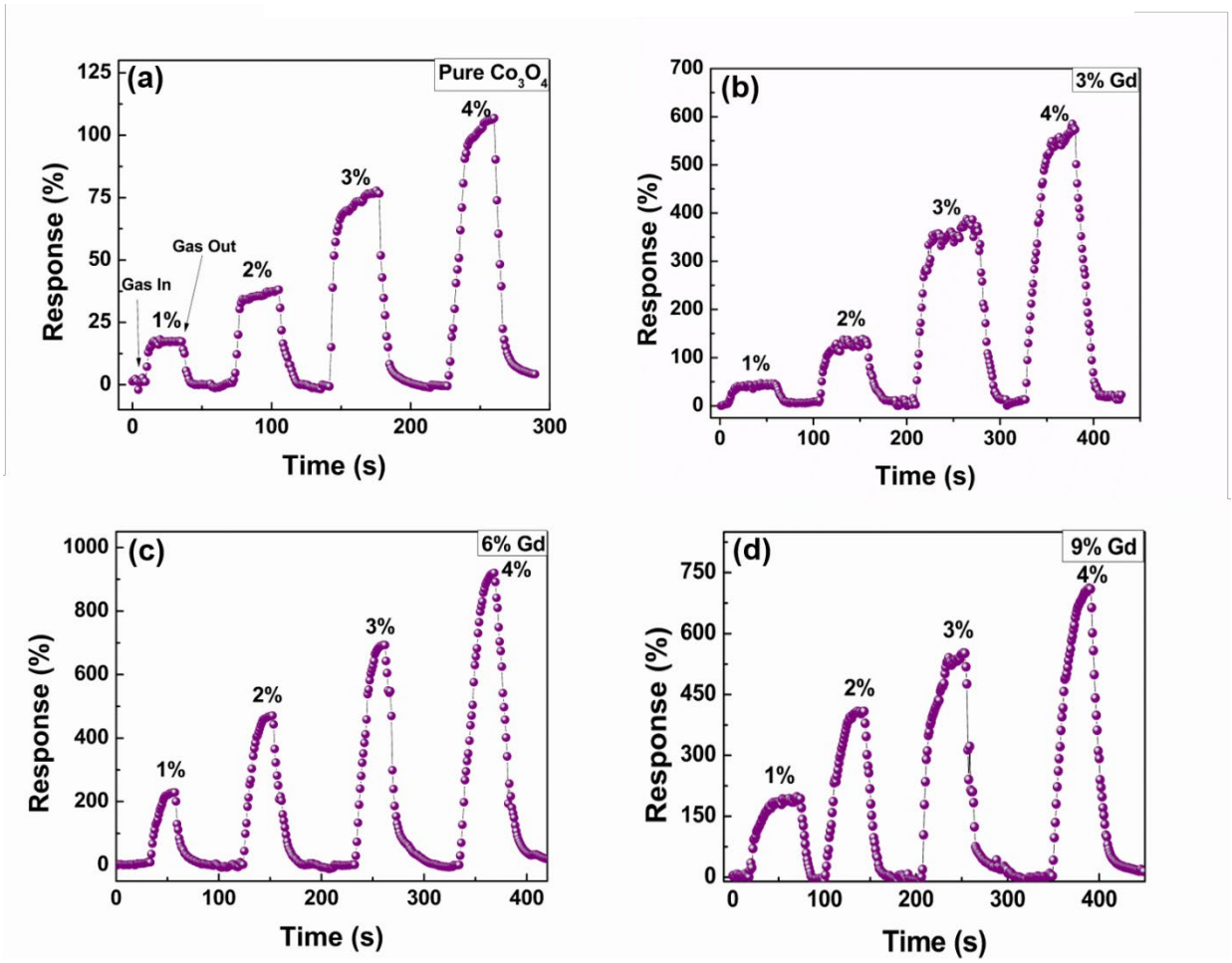

Figure 7 Response recovery transient of (a) pure Co_3O_4 (b) 3% Gd (c) 6% Gd and (d) 9% Gd doped Co_3O_4 in 1%, 2%, 3% and 4% oxygen concentration at 240 ℃

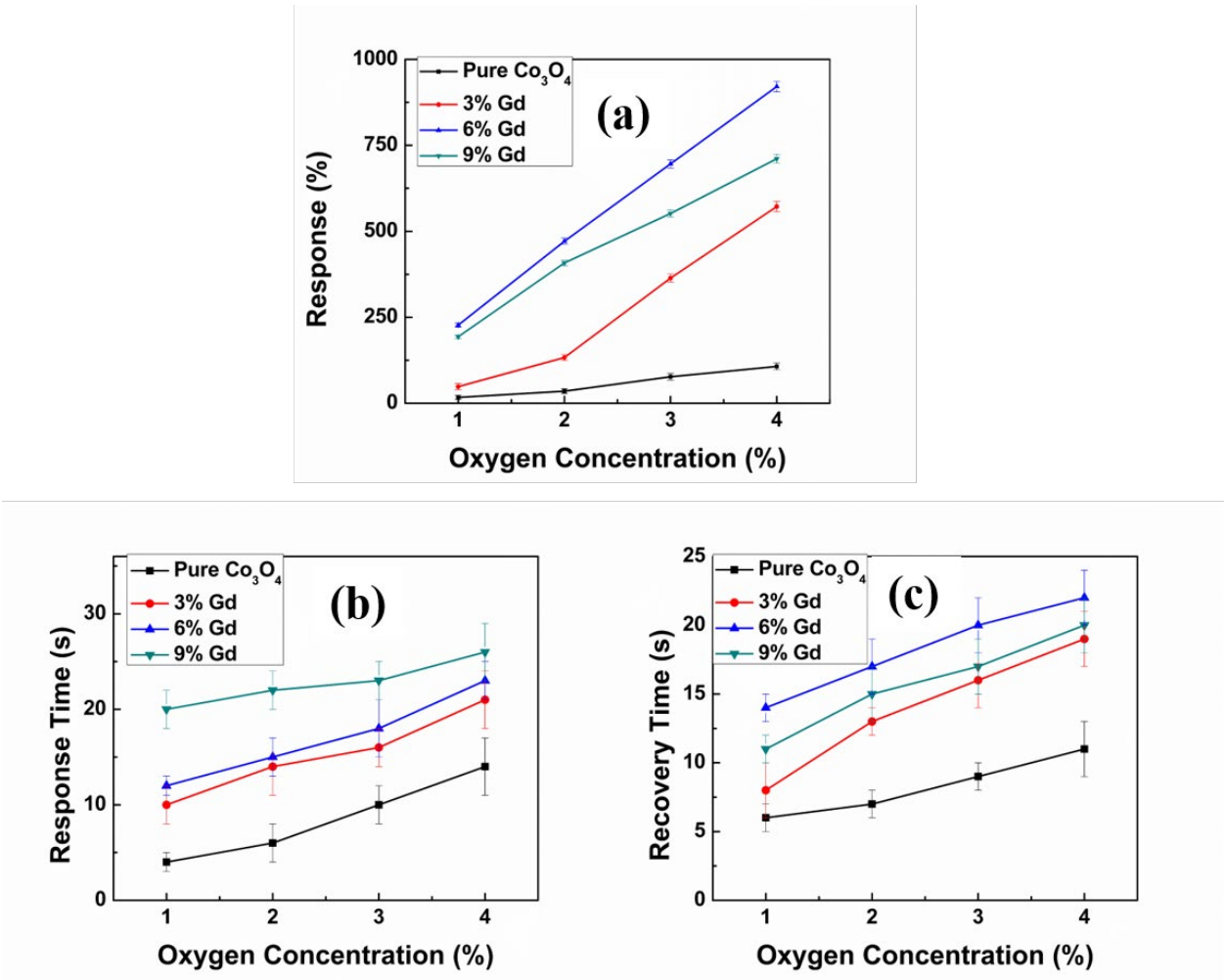

Figure 8 (a) Response (b) Response time and (c)Recovery time of sensors as a function of oxygen concentration at 240 ℃

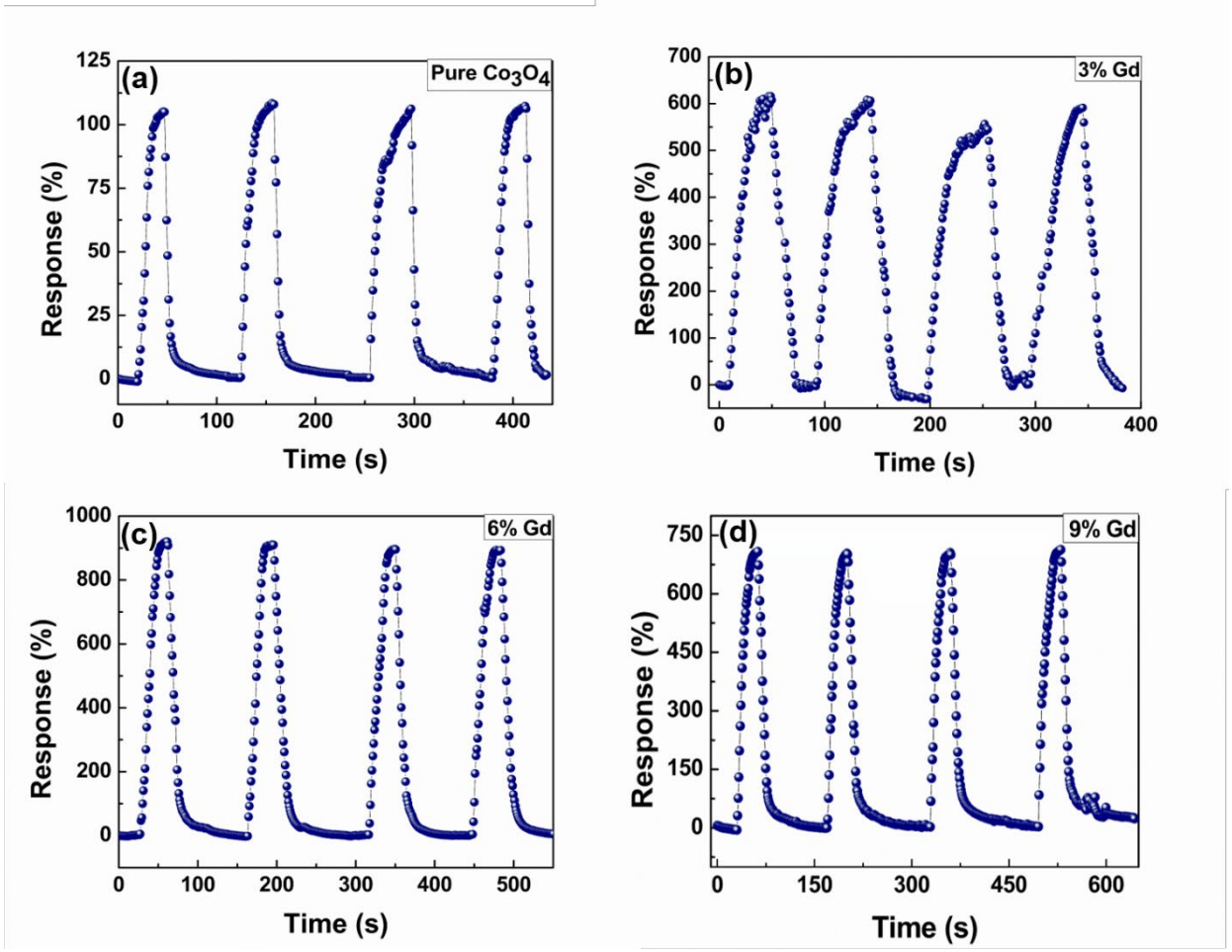

Figure 9 Continuous response recovery transient of (a) pure Co_3O_4 (b) 3% Gd (c) 6% Gd and (d) 9% Gd doped Co_3O_4 nanoparticles sensor in 4% oxygen concentration at 240 ℃

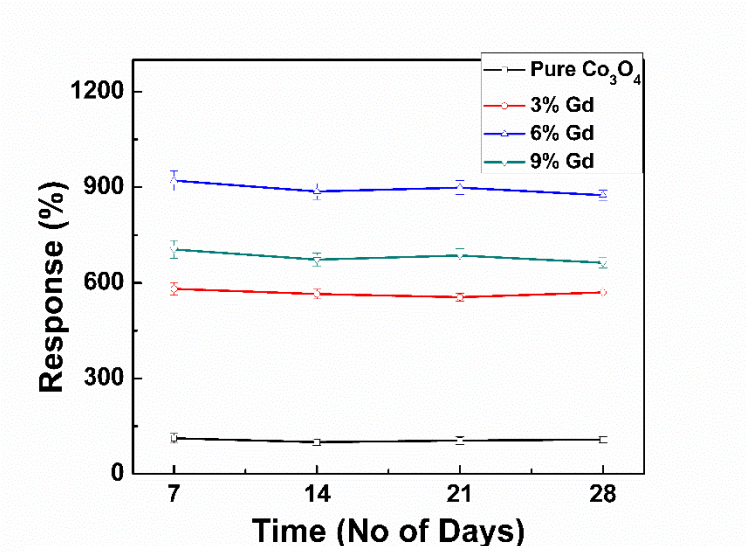

Figure 10 Stability of response of sensors measured at 240 ℃ in 4% Oxygen concentration

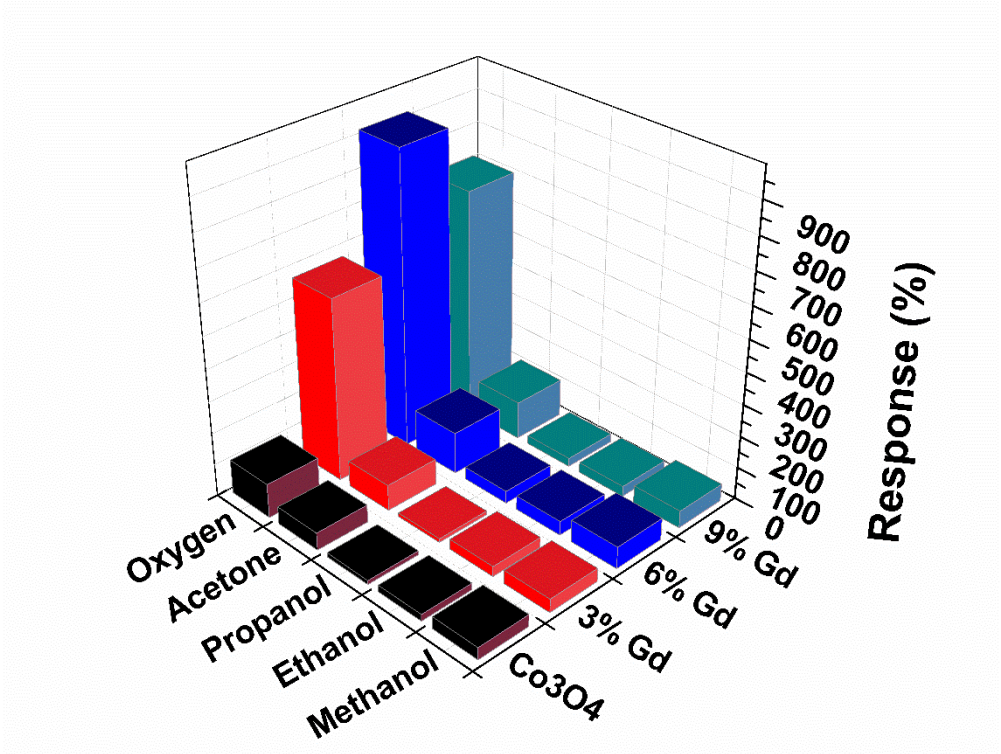

Figure 11 Response of sensors in 4% concentration of different gases at 240 ℃